

# Further Characterization of 394-GHz Gyrotron FU CW GII with Additional PID Control System for 600-MHz DNP-SSNMR Spectroscopy

Keisuke Ueda<sup>1</sup> · Yoh Matsuki<sup>1</sup> · Toshimichi Fujiwara<sup>1</sup> ·  
Yoshinori Tatematsu<sup>2</sup> · Isamu Ogawa<sup>2</sup> · Toshitaka Idehara<sup>2</sup>

Received: 22 February 2016 / Accepted: 18 April 2016 /  
Published online: 23 April 2016  
© Springer Science+Business Media New York 2016

**Abstract** A 394-GHz gyrotron, FU CW GII, has been designed at the University of Fukui, Japan, for dynamic nuclear polarization (DNP)-enhanced solid-state nuclear magnetic resonance (SSNMR) experiments at 600-MHz <sup>1</sup>H resonant frequency. After installation at the Institute for Protein Research (IPR), Osaka University, Japan, a PID feedback control system was equipped to regulate the electron gun heater current for stabilization of the electron beam current, which ultimately achieved stabilization of output power when operating in continuous wave (CW) mode. During exploration to further optimize operating conditions, a continuous tuning bandwidth of approximately 1 GHz was observed by varying the operating voltage at a fixed magnetic field. In the frequency range required for positive DNP enhancement, the output power was improved by increasing the magnetic field and the operating voltage from their initial operational settings. In addition, fine tuning of output frequency by varying the cavity cooling water temperature was demonstrated. These operating conditions and ancillary enhancements are expected to contribute to further enhancement of SSNMR signal.

**Keywords** Gyrotron · DNP · Solid-state NMR · PID control · Frequency tunability

---

✉ Keisuke Ueda  
keisuke.ueda.jp@gmail.com

<sup>1</sup> Institute for Protein Research (IPR), Osaka University, Yamadaoka 3-2, Suita-shi, Osaka-fu 565-0871, Japan

<sup>2</sup> Research Center for Development of Far-Infrared Region, University of Fukui (FIR UF), Bunkyo 3-9-1, Fukui-shi, Fukui-ken 910-8507, Japan

## 1 Introduction

### 1.1 Existing Gyrotrons for DNP-SSNMR

In the past decade, gyrotrons at 140, 250, 330, 460, and 527 GHz were developed for DNP-SSNMR at MIT [1–5]. The gyrotrons at 330 and 460 GHz have tuning bandwidths of >1 GHz and produce ~20 W of maximum power and more than ~5 W of average power. These gyrotrons continuously oscillated in second-harmonic  $TE_{3,4}$  and  $TE_{11,2}$  modes at 330 and 460 GHz, respectively. For low-loss transmission from the gyrotron to the NMR probe through waveguides, the output mode was converted to a Gaussian-like mode using an internal mode converter. The recent gyrotron at 527 GHz continuously produced ~20 W of output power in fundamental  $HE_{11}$  mode.

In addition, other gyrotrons for DNP-SSNMR were developed in the Research Center for Development of Far-Infrared Region, University of Fukui (FIR UF), Japan. The first practical gyrotron FU CW II at 394 GHz operated a CW output beam in the second-harmonic  $TE_{0,6}$  mode and achieved the world's first 600-MHz DNP-SSNMR at IPR in Osaka University, Japan [6–9]. In the experimental period, the field of the NMR magnet was swept with varying coil currents to investigate DNP enhancement factors and optimize the frequency matching conditions. However, this experiment quickly became an extended project, largely due to increased costs from liquid helium consumption.

To increase efficiency, a frequency-tunable gyrotron, FU CW VI, was tested in DNP-SSNMR experiments, instead of sweeping the magnetic field of the NMR magnet [10–12]. To cover the 600-MHz range of the positive and negative DNP enhancement maxima, a tuning bandwidth wider than 1 GHz was easily achieved by varying the main magnetic field strength. The observed CW output beam was changed from 394.4 to 395.6 GHz in the  $TE_{0,6}$  fundamental harmonic mode. However, the complex structures of those output beams were cylindrical and exhibited low power on the central axis, which is not suitable for efficient transmission through a waveguide.

Thus, in an effort to generate a circular radiation pattern of the output beam, a quasi-optical mode converter was incorporated into a gyrotron, FU CW GII [13, 14]. This gyrotron is of a vacuum-sealed type for easy vacuum maintenance and it operates in the second-harmonic  $TE_{8,3}$  mode in the cavity to generate a suitable frequency. The output beam patterns at the window were shown to include an effective Gaussian beam content. After satisfactory experimental operation at FIR UF, this gyrotron was installed in IPR for 600-MHz DNP-SSNMR spectroscopy.

Most recently, 460-GHz Gaussian beam gyrotrons, FU CW GO-I and GO-II, were developed for 700-MHz DNP-SSNMR spectroscopy [15]. Shortly thereafter, a frequency modulation function was added to keep the DNP enhancement factor at a high value [16].

### 1.2 The Present Study

Here, we report further characteristic evaluations of FU CW GII at IPR. Although the operation test was already performed at FIR UF, a more delicate adjustment was required than the initial operation test. To stabilize the output power and frequency, we applied a PID feedback control system to the cathode heater current, to stabilize the electron beam current. In examinations related to DNP resonance condition, we found a continuous tuning bandwidth of approximately 1 GHz by varying a cathode voltage at a fixed magnetic field of 7.22 T. However, the output power also varied throughout the frequency tuning. In particular, the power level in the higher-

frequency region, from 394.4 to 394.6 GHz, was much lower, which corresponds to the positive enhancement of our DNP experiments [11]. This condition was unable to satisfy the requirement of a DNP resonance condition. Eventually, this led to further exploration of parameters required for obtaining enough power within the optimal frequency range.

Here, we describe the effect of increasing the magnetic field and cathode voltage simultaneously for improvement in output power with the same oscillation mode. In addition, we describe another frequency change caused by thermal expansion of the cavity and demonstrate a fine tuning of frequency by varying the cavity cooling water temperature.

## 2 Necessity of Gyrotron for DNP-SSNMR

NMR is used for multiple molecular structural studies in atomic resolution. In particular, high-field SSNMR is widely used for structural studies of membrane proteins as drug targets [17], fibril proteins related to Alzheimer's disease [18], and microporous materials [19]. However, a significant limitation to SSNMR is that as molecules become larger, the signal sensitivity decreases because the number of target atoms per unit volume decreases. For example, each  $^{13}\text{C}$  NMR signal intensity of a larger molecule, such as amino acid, is weaker than that of a small molecule such as methanol. In the case of a large protein, signal detection is often limited and the measurement time can be over a week for integration of the spectrum.

DNP is an effective strategy for increasing sensitivity in order to overcome this limitation [20, 21]. This process is based on a large transfer of polarization from unpaired electron spins to nuclear spins. At the same temperature and magnetic field, the polarization of electron spins is larger than that of nuclear spins because the magnetic moment of electron spins is approximately three orders of magnitude larger than that of nuclear spins. When this transfer is successful, an increase of NMR signal intensity is achieved.

To perform DNP experiments in the solid state, large electron spin polarization should be saturated by exciting ESR transition. In our experiments at 14 T, or 600 MHz for  $^1\text{H}$  magnetic resonance, a stable paramagnetic reagent was mixed in a sample matrix as a source of unpaired electron spins [22].

For the excitation of electron spins, the paramagnetic reagent requires a sub-THz wave irradiation of 394 GHz by more than  $\sim 5$  W, which corresponds to the Larmor frequency of an electron at 14 T. Recently, high-frequency gyrotrons in the  $10^{11}$ – $10^{12}$  Hz band were successfully developed as a sub-THz wave source with an output of 100 W. More importantly, DNP experiments require frequency tunability to optimize frequency matching conditions between  $^1\text{H}$  spins and electron spins. Hence, the gyrotron is applied to DNP experiments.

## 3 Gyrotron Installation

The gyrotron FU CW GII was relocated from FIR UF to IPR and conditions necessary for safe and stable operation were created. The body was installed into an existing JASTEC liquid helium-free 8-T superconducting magnet (SCM), which had been used for a previous gyrotron, FU CW II. The evacuation of the gyrotron tube was performed by an ion pump to form a high vacuum condition of an order of  $10^{-6}$  Pa during operation. Part of the electron gun under the SCM was surrounded by three normal conducting coil magnets (gun coil). At the maximum current of 300 A, the magnetic field strength of the gun coil can be increased up to 0.19 T in

the center axis. A chilled water circulatory system with a cooling capacity of 1400 W was configured to remove heat from the electron beam collector and the gun coil. In addition, the resonator cavity needs to be precisely cooled during operation because the resonant frequency, output power, and mode pattern of the electron beam are affected by any slight change in the inner diameter of the cavity as a result of temperature change. Therefore, a separate chilled water circulator with a cooling capacity of 500 W (NesLab, RTE-17) was attached to cool the cavity. According to a previous study at FIR UF [14], the output frequency was slightly lower than our desired frequency region. Therefore, the temperature of the chiller was set at 4 °C which is lower than that in the previous study as a lower temperature is expected to contribute to a higher resonant frequency. To prevent a deviation from the set temperature, the water delivery tube was inserted into an Aerocel tube. To measure the temperature of the cavity, two thermocouple probes were placed on the outer wall surface of the cavity inlet and outlet ports.

The electron gun is of a triode type with an anode to provide optimum bias voltage and a cathode with a heating element (heater) to provide thermion. A high-voltage power supply for the cathode produces up to 500 mA of electron beam current and up to 30 kV of cathode voltage. To ensure safe operation without reaching the highest voltage, the main body of the cathodes' high-voltage power supply was located in a separate room. The controller for the cathode power supply and the other power supply bodies for the ion pump, anode, heater, gun coil, and SCM were mounted in a single 19-in. rack.

The operational state of the gyrotron was monitored and controlled by one laptop PC running NI LabVIEW. Three USB devices, NI USB 232, NI USB 6009, and NI USB 9211, were used to connect the laptop PC to each of the instruments. To reduce the influence of external noise, signal transmission lines from all instruments were connected via either optical fiber (i.e., with an RS232 converter for the heater power supply) or coaxial cables with the suitable grounding. NI USB 6009 and NI USB 9211 were incorporated in a terminal box with BNC connectors for high detachability. The BNC connectors were allocated to every channel of the USB devices as physical channels, and the channel alignment was programmable.

## 4 Experimental Results and Considerations

### 4.1 Performance of PID Control System

During operation or inspection, the output current and voltage from the cathode power supply (beam current  $I_b$  and cathode voltage  $V_k$ ), output current from the heater power supply (heater current  $I_h$ ), and vacuum pressure value were displayed and monitored via a PC laptop (LabVIEW software) (Fig. 1).

During usual operation of this gyrotron,  $I_b$  value often fluctuated in a regular period by less than  $\pm 5\%$ , although  $V_k$  was always stable. This fluctuation period was approximately 5 min and may be caused by a periodic temperature change in any part of the gyrotron or the laboratory room. In addition, as a response to the fluctuation of  $I_b$ , the output power of the sub-THz wave changes after a delay and fluctuates similarly to  $I_b$ . Therefore, the fluctuation of  $I_b$  needs to be suppressed efficiently.

In contrast, the temperature of the cathode and quantity of thermionically emitted electrons from the cathode vary only slightly after a delay with respect to the abrupt  $I_h$  variation. Therefore, even if  $I_h$  changes quickly while  $I_b$  is stable, a rapid change of the output power wave does not occur in the system. Therefore, the heater current was subjected to PID

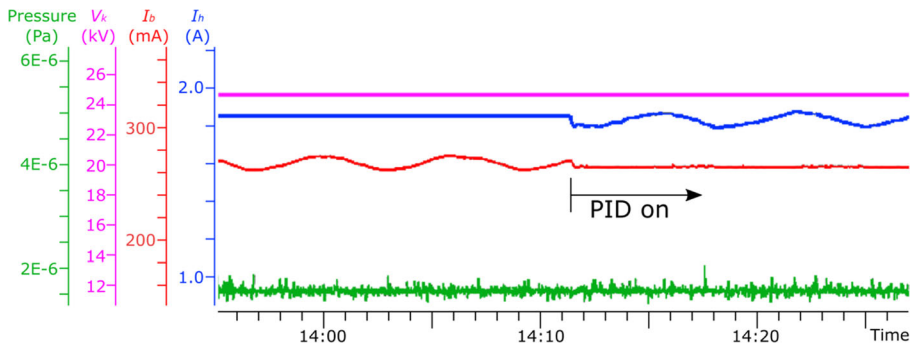


**Fig. 1** Stabilization of the electron beam current by a PID feedback control for heater current. During operation, four parameters are displayed on a LabVIEW chart: heater current  $I_h$  (blue), beam current  $I_b$  (red), cathode voltage  $V_k$  (cyan), and pressure (green)

feedback control in response to fluctuation in beam current. The block diagram of the PID feedback control of the gyrotron is shown in Fig. 2.

Using the virtual instrument in LabVIEW, the difference (as an error value) between a read value of  $I_b$  (process value) and a desired  $I_b$  (set value) was input and processed in the PID control circuit. The control variable value from the PID control circuit and a read  $I_h$  process value were added and output as a command signal of the output  $I_h$  that minimized the error value. After the PID control started, the fluctuation of  $I_b$  was stabilized and converged to be absorbed into  $I_h$  (Fig. 1).

According to a model of the gyrotron, a rapid fluctuation such as a spike in  $I_b$  is often observed. In such cases, the response time of the PID controller described here is not satisfactory. Therefore, the fluctuation of  $I_b$  and the resulting shift in output power cannot be reduced. To remove the rapid fluctuation, PID control of  $I_h$  for stabilization of  $I_b$  along with another PID control of the anode voltage for stabilization of the output power is effective [23, 24].

### 4.2 Frequency Tunability as Initial Design

The output frequency was measured using the heterodyne detection method. The radiated output wave (RF) from the window of the gyrotron was guided through waveguides and received by a rectangular horn antenna part of an even harmonic mixer (VDI WR 2.2 EHM). A local oscillation signal (LO) of approximately 24.65 GHz from a local signal generator

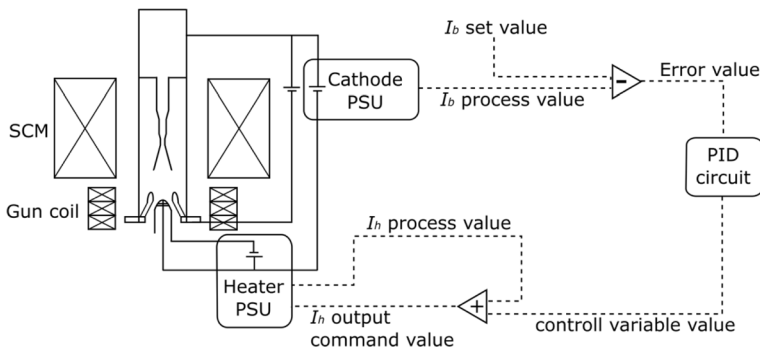


**Fig. 2** Block diagram of PID control system of  $I_b$  through feedback in heater power supply

(Agilent E8257D) was injected into the mixer part as a 16th harmonic for down-converting RF to an intermediate frequency signal (IF). Because IF contains two frequency components,  $RF - 16 \times LO$  and  $RF + 16 \times LO$ , both output IF peaks were explored on a spectrum analyzer/monitor (Agilent N1996A) by adjusting the LO frequency to decide the RF frequency.

The output power was measured at the front of the gyrotron window by calorimetric detection using water load equipment with a temperature sensor. The power in watts was calculated on the basis of the volume of water, irradiation time, and temperature difference between before and after exposure to the output wave. For more reliable measurements during the stabilization experiments, the frequency and power were measured after 5 min or longer from the completion of any parameter change.

For tuning the output frequency to a desired frequency, the field of the SCM is usually varied. However, because the threshold of the magnetic field that provides our desired frequency range is narrower in this system, fine tuning using the power supply of the SCM is difficult. In contrast, it is more convenient to achieve the frequency tuning by varying the operating voltage at a constant magnetic field than by varying the magnetic field at a constant voltage. Therefore, the output frequency tuning was performed by varying  $V_k$  at constant magnetic fields,  $B$ ; gun coil currents,  $I_g$ ; and anode voltages,  $V_a$ .

During the early stages of trial operations, we performed measurements within designated magnetic fields in accordance with previous reports [13, 14]. Figure 3 shows the measured frequency, output power, and calculated electron beam pitch factor [25] as a function of the operating  $V_k$  at the constant  $B = 7.22$  T. During the entire operation,  $I_b$  was maintained at 270 mA, which seems to be close to the limit for obtaining higher output power.

The continuously changing frequency range from 393.8 to 394.6 GHz was generated by varying  $V_k$  from  $-19$  to  $-15.3$  kV, respectively. Outside of the displayed range, the continuities

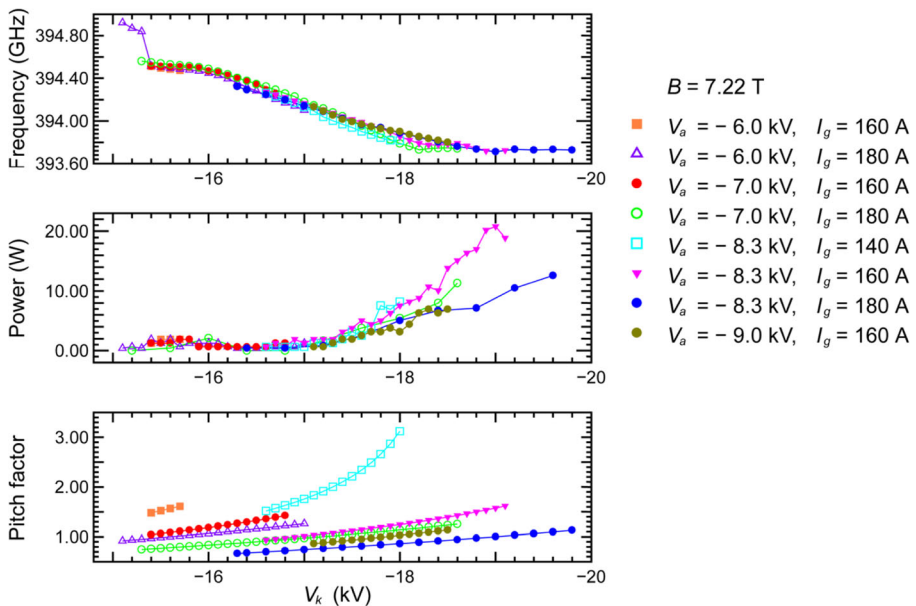


**Fig. 3** Measured frequency, power, and calculated pitch factor with respect to change in the cathode voltage  $V_k$ . The anode voltage  $V_a$  and the gun coil current  $I_g$  were set at a constant value. The magnetic field  $B$  of SCM was fixed at 7.22 T, and the electron beam current  $I_b$  was maintained at 270 mA

were lost, and output frequencies of other oscillation modes were sometimes observed. At the initial design stage, this gyrotron was optimized to perform stable oscillation with a frequency of approximately 394 GHz at  $B=7.2$  T [13, 14]. Based on the results of the frequencies, it seemed that the initial objective had been achieved. However, for the DNP experiment in current our NMR spectrometer, the power requirement is 5 W or more (at the front of the window), in the frequency range of 394.4 to 394.6 GHz. Although the target frequency range was achieved when varying  $V_k$  from  $-15.3$  to  $-16.4$  kV, the maximum output power was only 2.1 W.

To obtain more power in a simple manner,  $I_b$  may be increased by increasing  $I_h$ , which increases the quantity of thermions emitted from the cathode. Thus, when  $V_k$  was in the range of  $-15.3$  to  $-16.4$  kV,  $I_b$  was increased by changing the set value of  $I_b$  on the PID controller for each condition of  $V_a$  and  $I_g$ . Nevertheless, even when  $I_b$  was increased, the output power did not exceed 2.1 W. Moreover, the output power decreased and disappeared before  $I_b$  reached 300 mA in most experiments. It seems that the set value of approximately 270 mA was close to the limit for stable output power. The trial of larger  $I_b$  values than those previously used was no longer considered to be a viable option.

As an alternative strategy to obtain more power in the same mode, the pitch factor may be increased by increasing  $V_k$ . This was confirmed by the results of the performance test, shown in Fig. 3. However, the increase in  $V_k$  causes an increase in the vertical velocity ratio of the circular electron beam and contributes to a decrease in the oscillation frequency [25]. Therefore, the frequency deviates from the target frequency range of 394.4 to 394.6 GHz. Moreover, the spread of both the velocity and the electron distribution increases, which leads to distortion in the electron beam. This phenomenon caused output restrictions, and the output wave actually disappeared at one point.

### 4.3 Improvement of Output Power in a High-Frequency Region

To obtain enough output power within the target frequency range, we again focused on the relationships among  $V_k$ ,  $B$ , and frequency. An increase in  $V_k$  contributes to a decrease in frequency, whereas an increase in  $B$  contributes to an increase in frequency. This happens because the higher  $B$  contributes to an increase in the rotating velocity of the circular electron beam and a decrease of the electron beam radius. In addition, it maintains the quality of the electron beam at the higher  $V_k$ . Therefore, an increase in both  $V_k$  and  $B$  could be highly effective in increasing the output power while preventing a decrease in the frequency. However, in the same oscillation mode, as  $B$  is gradually increased from the initial design values, the continuous frequency tunable range obtained by varying  $V_k$  seems to narrow gradually. By recognizing this behavior, we further explored the optimal conditions for DNP experiments.

By increasing the value of  $V_k$  until it reached  $-29$  kV, while holding  $B$ ,  $V_a$ , and  $I_g$  at a constant value and maintaining  $I_b=270$  mA, the output power in a high-frequency region at a higher  $B$  was increased by more than that at a lower  $B$  (Fig. 4). However, the output wave of a low-frequency region at a higher  $B$  gradually disappeared. The continuously tunable ranges of the frequency at the higher  $B$  became narrower in comparison to the tunable ranges at the lower  $B$ . To keep the continuity of the output wave of the same mode,  $V_a$  was required to increase while increasing  $V_k$  and  $B$ . While higher  $V_k$  and  $B$  values should be tried, the limit value of  $V_k$  for the cathode power supply is fixed at  $-30$  kV. Therefore, the continuous frequency tunability at  $B=7.40$  T seems to be the approximate upper limit for increasing frequency and power simultaneously. Furthermore, this region, which has  $B=7.40$  T and  $V_k=-29$  kV, seems to be close to the limit for holding the same oscillation mode.



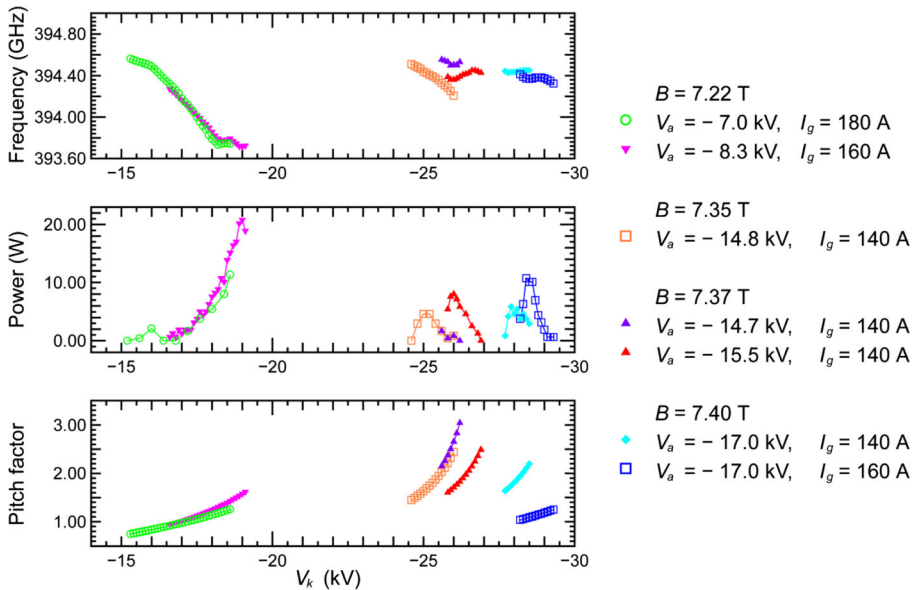


**Fig. 4** Transition of frequency tunability at various fixed values of  $B$ . During the operation,  $V_a$  and  $I_g$  were set to constant values, and  $I_b$  was maintained at 270 mA. Abbreviations are shown in Fig. 3

As reasonable evidence of this conclusion, a distinct phenomenon was observed. When an attempt was made to increase  $B$  at the constant  $V_k$  of approximately  $-29 \text{ kV}$ , the output wave disappeared and then reappeared. When the output wave reappeared, although the output power was high enough, the frequency was  $>398 \text{ GHz}$  and out of the target range. This appears to be another oscillation mode that has been previously reported [14].

Although the oscillation condition reaches its limit at  $B=7.40 \text{ T}$ , other conditions are satisfied, including both desired frequency and required power (Figs. 4 and 5). At some points, an output power of more than  $5 \text{ W}$  was obtained within the target frequency range of  $394.4$  to  $394.6 \text{ GHz}$ . In addition, some long-term stable oscillations were observed while both the frequency and power were held stable. For example, stable oscillations were observed for  $5 \text{ h}$  or longer when  $V_k=-27.9 \text{ kV}$ ,  $V_a=-17.0 \text{ kV}$ , and  $I_g=140 \text{ A}$  and when  $V_k=-27.9 \text{ kV}$ ,  $V_a=-16.0 \text{ kV}$ , and  $I_g=160 \text{ A}$ . For these conditions, we increased and decreased the value of  $I_b$ , and observed that the output power did not increase or the output wave disappeared. However, these oscillation conditions can be adequately applied to our DNP experiment.

#### 4.4 Frequency Tunability by Cavity Thermal Expansion and Contraction

Thermal tuning of the cavity radius is another useful strategy for frequency tuning. During operation, the temperature of the cavity was kept constant by the water chiller described in Section 3. An increase or decrease in the temperature of the cavity cooling water can expand or reduce the inner diameter of the cavity. Therefore, the diameter of the circular electron beam, which contributes to the output frequency, can be tuned by setting the temperature of the water chiller.

The correlation between the output frequency and changes in cavity outlet water temperature, in the range of  $8.6$  to  $24.1 \text{ }^\circ\text{C}$ , are shown in Fig. 6. The operation was performed under



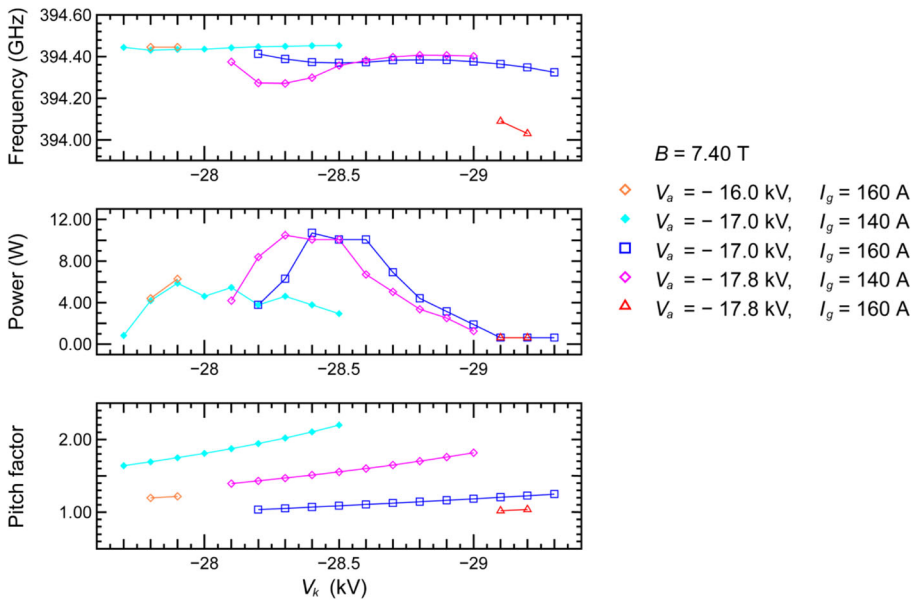


Fig. 5 Enlargement of Fig. 4 for  $B = 7.40$  T. Three additional conditions are shown

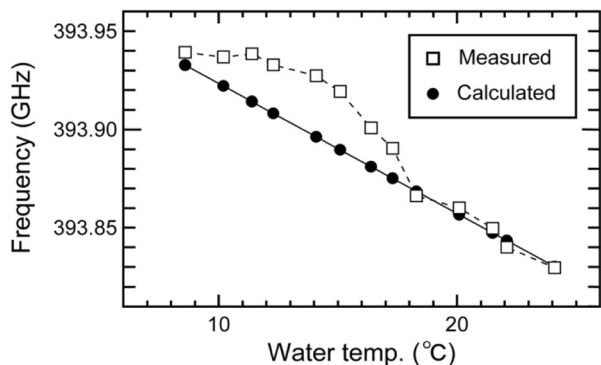
the condition of  $B = 7.22$  T,  $V_k = -17.8$  kV,  $V_a = -8.3$  kV,  $I_g = 160$  A, and  $I_b = 270$  mA, while varying the set temperature of the water chiller. Both the output frequency and outlet water temperature were measured after 10 min or longer from the time when the set temperature was altered. Measured frequency was observed to decrease in proportion to a rise in temperature. This relationship approximates to the theoretical frequency shift calculated in previous publications [26, 27]. The calculation method is as follows:

The cavity exchanges heat with the flowing cooling water. Therefore, the quantity of heat,  $Q$ , of the cooling water is approximated as power,  $P$ , and is given by the following equation:

$$Q \approx P = c\rho q_v(T_2 - T_1)$$

where  $c$  is the specific heat capacity,  $\rho$  is the density,  $q_v$  is the volumetric flow rate, and  $T_1$  and  $T_2$  are the inlet and outlet cooling water temperatures, respectively.

Fig. 6 Frequency change with respect to cavity cooling water temperature



The cavity part can be considered as a simple tube. Therefore, the temperature-dependent cavity radius  $r$  is approximately given by the following equation:

$$r = r_0\{1 + \alpha(T_3 - T_1)\}$$

where  $r_0$  is the radius of the cavity at 0 °C,  $\alpha$  is the thermal expansion coefficient of the material, and  $T_3$  is the cavity inner wall temperature.

From the solution of the steady-state heat conduction equation, the relationship between  $T_2$  and  $T_3$  is shown in the following equation:

$$T_3 = T_2 - \frac{Q}{2\pi\kappa l_c} \ln\left(\frac{r_1}{r_2}\right)$$

where  $\kappa$  is the thermal conductivity,  $l_c$  is the length of the cavity, and  $r_1$  and  $r_2$  are the radii of the inner and outer walls of the cavity, respectively.

The relationships among the changes in the frequency, cavity radius, and temperature are denoted by the following equation:

$$\frac{f - f_0}{f_0} = \frac{r_0 - r}{r_0} = -\alpha(T_3 - T_1)$$

where  $f$  and  $f_0$  are the oscillation frequency for the radii of  $r$  and  $r_0$ , respectively.

Thus, we derive the following frequency equation:

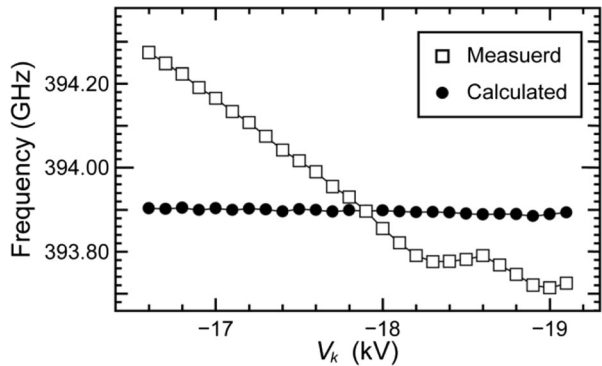
$$f = f_0\{1 - \alpha(T_3 - T_1)\}$$

In this experiment, the observed frequency tunability was approximately 0.1 GHz and the output power showed little or no change. This is probably because the frequency range was not as wide as the ranges used for the experiment shown in Fig. 3. In the range of 10.2 to 17.3 °C (Fig. 6), the deviation between measured and calculated frequency was slightly larger compared with that in the range of 18.3 to 24.1 °C. This deviation is probably due to an unstable state of heat balance in the cavity while varying the set temperature. Theoretically, the frequency tuning range could be widened by further increasing or decreasing the set temperature. However, we limited the temperature range, as shown in Fig. 6, to protect against dew condensation by excessive cooling or from damage by excessive heating. With such limitations (by far the most common), the frequency tunability becomes smaller than the frequency tunability by  $V_k$  or  $B$ . However, for existing gyrotron tubes, fine tuning of the frequency can be easily performed without complicated electric wiring and machining. Therefore, if coarse tuning is not required, this easy method can be employed in other gyrotron tubes of the same type.

Thus, frequency is tunable by varying cooling water temperatures, although it can also be tuned by varying  $V_k$ , as mentioned above (Figs. 3, 4, and 5). However, the cooling water temperature can be changed by various external factors. These results raise questions as to whether frequency can be influenced by cooling water temperature while varying  $V_k$ .

To address this question, when the frequency was measured while varying  $V_k$ , the cooling water temperature was also recorded. Then, the theoretical frequency was calculated from the cooling water temperature and compared against the measured frequency. Figure 7 shows an example in which the calculated frequency is compared

**Fig. 7** Influence of the cavity cooling water temperature on the frequency while varying  $V_k$



with the measured frequency when  $B=7.22$ ,  $V_a=-8.3$  kV,  $I_g=160$  A, and  $I_b=270$  mA, which corresponds to the results in Figs. 3 and 4. At that time, the temperature differences in the cooling water between the inlet and outlet ports were in the range of 3.5 to 5.4 °C. In this temperature range, the calculated frequency fluctuated in the range of only 0.02 GHz, while the measured frequency changed in the range of approximately 0.6 GHz. Moreover, all the temperature differences between inlet and outlet ports in the other experiments described above were less than 6 °C. Therefore, under such conditions, the oscillation frequency is practically dominated by  $V_k$  and is hardly affected by the slight change in the cooling water temperature.

## 5 Summary

In previous publications regarding gyrotron FU CW GII [13, 14], the changes in frequencies, output power, oscillation mode patterns, and radiation patterns were measured for a wide magnetic field range. However, in a narrow frequency range for a DNP resonant condition, more satisfactory conditions have not yet been thoroughly investigated. This led us to explore optimal parameters for DNP experiments.

In this study, a novel PID feedback control system for electron gun heater current stabilization of electron beam current was incorporated into the relocated FU CW GII from FIR UF. This PID control system can negate fluctuations in the electron beam that can cause deviation of output power.

During operation, at a fixed magnetic field of 7.22 T, a continuous frequency tunability from 393.7 to 394.6 GHz is achieved by varying the operating voltage. With a higher magnetic field and higher operating voltage, the lower frequency region disappears, whereas the higher frequency region obtains more power. Between 394.4 and 394.6 GHz at 7.40 T, which corresponds to the frequency range of the positive DNP enhancement, the output power exceeded 5 W for the first time. Furthermore, it was demonstrated that it is possible to fine tune output frequency by varying the cavity cooling water temperature. These operating conditions satisfy the conditional requirements of our current 600-MHz DNP-SSNMR spectrometer and promise to contribute to long-term stable measurement.

**Acknowledgments** This work was partially supported by the SENTAN project of JST, Grant in Aid for Scientific Research (B) (no. 24360134) from the Japan Society for Promotion of Science (JSPS), and the Targeted Proteins Research Program of MEXT.

We are grateful to Dr. Alexei Kuleshov and Dr. Eduard Khutoryan from O. Ya. Usikov Institute of Radio Physics and Electronics, National Academic of Science Ukraine, for the discussion about PID control.

We would like to thank M. Tomohiro Kanemaki from the Research Center for Development of Far-Infrared Region, University of Fukui, for helping during the fabrication of the components.

We would also like to thank our colleague Dr. Kris Frost for the English language review.

## References

1. S.-T. Han, R. G. Griffin, K.-N. Hu, C.-G. Joo, C. Joye, J. R. Sirigiri, R. J. Temkin, A. Torrezan, and P. Woskov, *IEEE Trans Plasma Sci IEEE Nucl Plasma Sci Soc*, **35**, 559 (2007)
2. V. S. Bajaj, M. Hornstein, K. Kreisler, J. Sirigiri, P. Woskov, M. Mak-Jurkauskas, J. Herzfeld, R. Temkin, and R. Griffin, *J Magn Reson*, **189**, 251 (2007)
3. C. Torrezan, M. A. Shapiro, J. R. Sirigiri, R. J. Temkin, and R. G. Griffin, *IEEE Trans Electron Devices*, **58**, 2777 (2011)
4. C. Torrezan, S.-T. Han, I. Mastovsky, M. A. Shapiro, J. R. Sirigiri, R. J. Temkin, A. Barnes, and R. Griffin, *IEEE Trans Plasma Sci IEEE Nucl Plasma Sci Soc*, **38**, 1150 (2010)
5. S.K. Jawla, W.C. Guss, M. A. Shapiro, and R. J. Temkin, *IRMMW-THz*, (2014) doi:10.1109/IRMMW-THz.2014.6956164.
6. T. Idehara, I. Ogawa, L. Agusu, T. Kanemaki, S. Mitsudo, T. Saito, T. Fujiwara, and H. Takahashi, *Int J Infrared Milli Waves*, **28**, 433 (2007)
7. L. Agusu, T. Idehara, I. Ogawa, T. Saito, T. Kanemaki, H. Takahashi, and T. Fujiwara, *Int J Infrared Milli Waves*, **28**, 499 (2007)
8. T. Idehara, T. Saito, I. Ogawa, S. Mitsudo, Y. Tatematsu, L. Agusu, H. Mori, and S. Kobayashi, *Appl Magn Reson*, **34**, 265 (2008)
9. Y. Matsuki, H. Takahashi, K. Ueda, T. Idehara, I. Ogawa, M. Toda, H. Akutsu, and T. Fujiwara, *Phys Chem Chem Phys*, **12**, 5799 (2010)
10. T. Idehara, K. Kosuga, L. Agusu, R. Ikeda, I. Ogawa, T. Saito, Y. Matsuki, K. Ueda, and T. Fujiwara, *J Infrared Milli Terahz Waves*, **31**, 775 (2010)
11. Y. Matsuki, K. Ueda, T. Idehara, R. Ikeda, K. Kosuga, I. Ogawa, S. Nakamura, M. Toda, T. Anai, and T. Fujiwara, *J Infrared Milli Terahz Waves*, **33**, 745 (2012)
12. Y. Matsuki, K. Ueda, T. Idehara, R. Ikeda, I. Ogawa, S. Nakamura, M. Toda, T. Anai, and T. Fujiwara, *J Magn Reson*, **225**, 1 (2012)
13. Y. Tatematsu, Y. Yamaguchi, T. Idehara, T. Kawase, R. Ichioka, I. Ogawa, T. Saito, and T. Fujiwara, *J Infrared Milli Terahz Waves*, **35**, 169 (2014)
14. Y. Tatematsu, Y. Yamaguchi, T. Idehara, T. Kawase, I. Ogawa, T. Saito, and T. Fujiwara, *J Infrared Milli Terahz Waves*, **35**, 517 (2014)
15. T. Idehara, Y. Tatematsu, Y. Yamaguchi, E. M. Khutoryan, A. N. Kuleshov, K. Ueda, Y. Matsuki, and T. Fujiwara, *J Infrared Milli Terahz Waves*, **36**, 613 (2015)
16. T. Idehara, E. M. Khutoryan, Y. Tatematsu, Y. Yamaguchi, A. N. Kuleshov, O. Dumbrajs, Y. Matsuki, and T. Fujiwara, *J Infrared Milli Terahz Waves*, **36**, 819 (2015)
17. A. Watts, *Nat Rev Drug Discov*, **4**, 555 (2005)
18. R. Tycko, *Q Rev of Biophys*, **39**, 1 (2006)
19. S. Ashbrook, D. Dawson, and V. Seymour, *Phys Chem Chem Phys*, **16**, 8223 (2014).
20. A. Abragam and M. Goldman, *Reports on Progress in Physics*, **41**, 395 (1978)
21. K.-N. Hu, G. Debelouchina, A. Smith, and R. Griffin, *J Chem Phys*, **134**, 125105 (2011)
22. C. Song, K.-N. Hu, C.-G. G. Joo, T. M. Swager, and R. G. Griffin, *J Am Chem Soc* **128**, 11385 (2006)
23. T. Idehara, A. N. Kuleshov, K. Ueda, and E. M. Khutoryan, *J Infrared Milli Terahz Waves*, **35**, 159 (2014)
24. E. M. Khutoryan, T. Idehara, A. N. Kuleshov, and K. Ueda, *J Infrared Milli Terahz Waves*, **35**, 1018 (2014)
25. S. E. Tsimring, *Int J Infrared Milli Waves*, **22**, 1433 (2001)
26. T. Idehara, Y. Iwata, and I. Ogawa, *Int J Infrared Milli Waves*, **24**, 119 (2003)
27. T. Hori, T. Idehara, H. Sasagawa, A. Kimura, I. Ogawa, and S. Mitsudo, *Rev Sci Instrum* **76**, 023502 (2005)